A&A 378, 509–521 (2001)
DOI: 10.1051/0004-6361:20011201

Astronomy & Astrophysics

Neutron-capture and 2.22 MeV emission in the atmosphere of the secondary of an X-ray binary

P. Jean[1] and N. Guessoum[2]

[1] Centre d'Étude Spatiale des Rayonnements, CNRS/UPS, 9 avenue du colonel Roche, 31028 Toulouse, France
e-mail: jean@cesr.fr
[2] American University of Sharjah, College of Arts & Sciences, Physics Unit, Sharjah, UAE
e-mail: nguessoum@aus.ac.ae

Received 11 May 2001 / Accepted 8 August 2001

Abstract. We consider the production of 2.22 MeV radiation resulting from the capture of neutrons in the atmosphere of the secondary in an X-ray binary system, where the neutrons are produced in the accretion disk around the compact primary star and radiated in all directions. We have considered several accretion disk models (ADAF, ADIOS, SLE, Uniform-Temperature) and a varity of parameters (accretion rate, mass of the compact object, mass, temperature and composition of the secondary star, distance between the two objects, etc.). The neutron rates are calculated by a network of nuclear reactions in the accretion disk, and this is handled by a reaction-rate formulation taking into account the structure equations given by each accretion model. The processes undergone by the neutrons in the atmosphere of the companion star are studied in great detail, including thermalization, elastic and inelastic scatterings, absorption, escape from the surface, decay, and capture by protons. The radiative transfer of the 2.22 MeV photons is treated separately, taking into consideration the composition and density of the star's atmosphere. The final flux of the 2.22 MeV radiation that can be detected from earth is calculated taking into account the distance to the source, the direction of observation with respect to the binary system frame, and the rotation of the source, as this can lead to an observable periodicity in the flux. We produce phasograms of the 2.22 MeV intensity as well as spectra of the line, where rotational Doppler shift effects can lead to changes in the spectra that are measurable by INTEGRAL's spectrometer (SPI).

Key words. X-rays: binaries – accretion, accretion disks – gamma-ray: theory – lines: profiles – nuclear reactions, nucleosynthesis, abundances

1. Introduction

The capture of a neutron by a proton and the subsequent emission of a photon at 2.223 MeV has been the object of much interest since the dawn of gamma-ray astrophysics (Fichtel & Trombka 1981) because it represents a potentially important spectroscopic tool in the investigation of high-energy environments such as solar flares, neutron star surfaces or accretion disks around compact objects. Several studies have been conducted both from theory and observation, realizing that this line is the most promising candidate of all nuclear gamma-ray processes.

Solar flares have had the lion's share of works because of the obvious possibilities of detailed investigation: Hua & Lingenfelter (1987), Murphy et al. (1991), Share & Murphy (1995), Ramaty et al. (1995), Ramaty et al. (1996); and others. Other sources have also been investigated, although no detection has been confirmed and established to date, despite several previous announcements (Jacobson 1982; McConnell et al. 1997).

Send offprint requests to: P. Jean,
e-mail: Pierre.jeau@cesr.fr

On the theoretical front, Guessoum & Dermer (1988) conducted a detailed theoretical investigation in the context of compact binary sources, taking Cygnus X-1 as a case-study and pointing out the possibility of emission of a very narrow 2.22 MeV line from the atmosphere of the companion, while Aharonian & Sunyaev (1984) had considered a two-temperature accretion disk and considered the possibility of emission from the disk itself, where the line would be very broad. Bildsten and co-workers considered the possibility of emission at the surface of a neutron star, as a result of bombardment by accreted protons (Bildsten 1991; Bildsten et al. 1993). In the same framework, Bykov et al. (1999) recently considered the possibility of detecting nuclear gamma-ray lines from accreting objects with INTEGRAL. Vestrand (1989) investigated the 2.22 MeV emission resulting from very high energy ($E > 10^{12}$ eV) protons bombarding companion stars of sources such as Cyg X-3, Vel X-1, and Her X-1, and predicted significant fluxes ($\approx 10^{-4}$ photons cm^{-2} s^{-1}). Finally, Guessoum & Kazanas (1999), interested in Lithium production by neutron bombardment of X-ray binary companions' atmospheres and using the ADAF

accretion disk model, estimated the flux of 2.22 MeV line emission from a source at about 1 kpc and found it generally very low (10^{-7} photons cm^{-2} s^{-1}).

On the observational front, extensive searches of the line have been conducted with the data from the Solar Maximum Mission (Harris & Share 1991) and the COMPTEL instrument of the Compton-GRO mission (McConnell et al. 1997). The latter showed an excess emission at $(l,\ b) = 300^{\rm o},\ -30^{\rm o}$ at about 3.7 σ. No obvious counterparts (X-ray binaries or the like) could be linked to that general direction, although a catalysmic variable has been suggested as a likely candidate for that emission. Van Dijk (1996) has compiled a list of upper-limit 2.22 MeV binary-source radiation fluxes based on COMPTEL observations of 27 black-hole candidates. These upper limits range from 1 to 5×10^{-5} photons cm^{-2} s^{-1}.

The production of neutrons in the accretion disks around the primaries of X-ray binaries is a direct result of the high temperatures that prevail in such environments. The gravitational attraction, combined with the viscous dissipation, leads to a significant heating of the plasma, particularly its nuclei, resulting in temperatures as high as 10^{10}–10^{12} K in the inner regions ($r \approx 1{-}100\ R_{\rm S}$, where $R_{\rm S} = 2GM/c^2$ is the Schwarzchild radius of the central compact object). Simple considerations show that densities of the accretion plasma can range between 10^{12} and 10^{18} cm^3 depending on the geometry and the model, which implies substantial nuclear reactions. Since the accreted material is expected to contained He and/or metals (depending on whether the secondary star's composition is normal or of Wolf-Rayet type), breakup reactions will produce significant amounts of neutrons. Part of the present paper is devoted to computing precisely such amounts under various assumptions: different accretion disk models, different initial compositions of the accreted material, different temperature profiles, etc. This will be presented in detail in Sect. 2.

There are several reasons underlying our interest in 2.22 MeV emission from the secondary stars of X-ray binaries. First and foremost, as mentioned above the CGRO 2.22 MeV map showed that there are real possibilities for the detection of this line, which would consitute the first observation of any nuclear gamma-ray line outside of the solar system, and this prospect is heightened by the upcoming INTEGRAL mission's order-of-magnitude improvement in both flux sensitivity and energy resolution, which become crucial when most predictions of line fluxes from such sources are at the 10^{-5} photons cm^{-2} s^{-1} level, that is below the sensitivity of CGRO and right at the detection threshold of INTEGRAL. Secondly, the accretion disk problem remains fully unresolved (very little progress has been made on the determination of the disk structure, much less the identification of the viscosity mechanism), and since our results will show significant differences in fluxes and therefore in the possibility for detection of this line emission, this may constitute further testing of models. Furthermore, we will find that line fluxes depend substantially on the secondary star's characteristics (elemental composition in particular), the eventual detection of such a signal would then also constitute a diagnostic of the X-ray binary's secondary (e.g. convection and mixing of the gas).

This paper is structured as follows: in Sect. 2, the treatment of neutron production in the accretion disk (and its subsequent escape) is presented for various models; in Sect. 3, the detailed treatment of neutron propagation, slow-down, and capture in the atmosphere of the secondary is shown; in Sect. 4 we present the results of line fluxes when everything is combined: neutron production and escape from the disk, various interactions and effects (geometrical as well as physical) in the atmosphere of the secondary, and finally capture and gamma-ray emission, with star rotation, photon energy shift, etc.; in the final section we discuss our results with INTEGRAL observation prospects in mind and point to future work on the subject.

2. Neutron production in the accretion disk

Neutrons are produced by means of nuclear breakup reactions involving hydrogen and helium nuclei. Once produced, the neutrons can escape or carry part of the angular momentum outward by collisions with the infalling nuclei, thereby participating in the viscous dissipation, as they are not affected by the presence of any magnetic fields. In fact, the escape of the neutrons from the gravitational attraction of the compact object can be computed quite accurately in the assumption of thermal conditions (Aharonian & Sunyaev 1984; Guessoum & Kazanas 1990). So, at least in principle, the calculation of the flux of neutrons irradiating the surface of the companion star is quite feasible. In practice, however, there are a number of factors which intervene and make the task somewhat more complicated: the temperature and density distribution of matter in the accretion disk is model-dependent, the composition and nuclear abundances of the plasma depends on stellar evolution conditions, and cross sections for the various reactions are not always known accurately (and this depends also on the extent of the nuclear reactions network taken into account in the computation).

Since the nuclear reactions relevant to our problem and to the production of gamma rays require energies of about 10 MeV per nucleus, our interest is limited to the inner regions of the accretion flow, i.e. regions around the compact object between about 100 Schwarzschild radii) and either the surface of the neutron star or the horizon of the black hole, depending on the nature of the compact object. For general purposes, we assume a mass of 1 $M_\odot$ for the compact object, unless a specific case is considered.

In this work we consider a number of relatively simple accretion disk models:

– 1 – The Advection-Dominated Accretion Flow (ADAF) model proposed by Narayan and co-workers (Narayan & Yi 1994; Chen et al. 1995; Narayan et al. 1995; Narayan & Yi 1995), which has the added appeal

that its temperature and density function are very simple and analytical expressions (Yi & Narayan 1997):

$$T_{\rm i} = 1.11 \times 10^{12}\, r^{-1}\ {\rm K} = 95.68\, r^{-1}\ \ {\rm MeV} \qquad (1)$$

where r is the dimensionless radial variable $r = R/R_{\rm S}$;

$$n = 6.4 \times 10^{18}\ \alpha^{-1}\ m^{-1}\ \dot{m}\ r^{-3/2}\ {\rm cm}^{-3} \qquad (2)$$

where m is the dimensionless mass measured in units of a solar mass ($m = M/M_{\odot}$), $\dot{m}$ is the dimensionless accretion rate measured in units of the Eddington accretion rate $\dot{m} = \dot{M}/\dot{M}_{\rm Edd} = \dot{M}/1.4 \times 10^{17} m$ g/s (in this work we will consider values of $\dot{M}$ in the range of $10^{-10}\ M_{\odot}$/yr–$10^{-8}\ M_{\odot}$/yr), taking β (the ratio of gas pressure to total pressure) to equal 1/2 (as in Yi & Narayan 1997); the central factor α is taken to equal either 0.3 or 0.1 (following Narayan & Yi 1994).
Furthermore, it must be noted that in this model the value of the electron temperature does not affect our results, which depend mainly on the profile of the ion temperature $T_{\rm i}(r)$.

– 2 – The Advection-Dominated Inflow-Outflow Solutions proposed by Blandford and Begelman (1998), which consist of a "generalized" ADAF model where only a small fraction of the gas initially supplied ends up falling onto the compact object, and where the energy released is transported radially outward and effectively becomes a wind, driving away the rest of the accreted material.
In this family of solutions, a central assumption is the radial dependence of the accretion rate as $\dot{m}(r) \propto r^{p}$, $0 \leq p < 1$. In the present work, we take the "gasdynamical wind" (case iv of Blandford & Begelman 1998) solution, i.e. $p = 1/2$, $\epsilon = 1/2$, which leads to a density function $n \propto r^{-1}$; more precisely:

$$n = 2.18 \times 10^{19}\ \alpha^{-1}\ \frac{(4.52 \times 10^{8}) \times \dot{M}}{mr}\ {\rm cm}^{-3}\ . \qquad (3)$$

Note that this special form of the density function also corresponds to the solution obtained by Kazanas et al. (1997) in fitting the time lags in similar, compact X-ray accreting sources.
Another important equation is that of the disk height h (in units of $R_{\rm S}$), which in the particular solution adopted here, is given by:

$$h = 0.447\ \times 3\, m\, r. \qquad (4)$$

Also, the radial velocity is

$$v_{\rm r} = 0.52\ \alpha\ r^{-\frac{1}{2}}\ c\ {\rm cm/s}. \qquad (5)$$

Finally, the ion temperature profile is the same as in ADAF.

– 3 – The Two-Temperature Shapiro-Lightman-Eardley (1976) Model, for which the expressions are given by:

$$T_{\rm i} = 5 \times 10^{11}\ M_{*}^{-\frac{5}{6}}\ \dot{M}_{*}^{\frac{5}{6}}\ \alpha^{-\frac{7}{6}}\ \phi^{\frac{5}{6}}\ r_{*}^{-\frac{5}{4}}\ {\rm K} \qquad (6)$$

$$T_{\rm e} = 7 \times 10^{8}\ M_{*}^{\frac{1}{6}}\ \dot{M}_{*}^{-\frac{1}{6}}\ \alpha^{-\frac{1}{6}}\ \phi^{-\frac{1}{6}}\ r_{*}^{\frac{1}{4}}\ {\rm K} \qquad (7)$$

$$h = 10^{5}\ M_{*}^{\frac{7}{12}}\ \dot{M}_{*}^{-\frac{5}{12}}\ \alpha^{-\frac{7}{12}}\ \phi^{\frac{7}{12}}\ r_{*}^{\frac{7}{8}}\ {\rm cm} \qquad (8)$$

$$\rho = 5 \times 10^{-5}\ M_{*}^{-\frac{3}{4}}\ \dot{M}_{*}^{-\frac{1}{4}}\ \alpha^{\frac{3}{4}}\ \phi^{-\frac{1}{4}}\ r_{*}^{-\frac{9}{8}}\ {\rm g/cm}^{3}, \qquad (9)$$

where $M_{*} = M/3; \phi = 1 - \sqrt{3R_{\rm S}/R} = 1 - \sqrt{3/r}; \dot{M}_{*} = \dot{M}/10^{17}{\rm g/s}; r_{*} = 2R/R_{\rm S} = 2r$.

– 4 – The uniform-temperature model, similar to the one used in the Guessoum & Kazanas (1990) neutron-viscosity model, where $T_{\rm i}$ is set by a viscosity condition but is taken to be uniform in the disk, and $T_{\rm e}$ is chosen arbitrarily (usually between 0.1 and 0.5 MeV); the density is then obtained from an energy balance requirement (viscous heating of the ions equal to Coulomb energy transfer from the ions to the electrons). In the Guessoum & Kazanas model, the following relations were derived:

$$n = \frac{3.375 \times 10^{25}}{r^{2}} \sqrt{\frac{\dot{m}}{m^{3}\, f_{\rm th}}} \qquad (10)$$

where $f_{\rm th}$ is the ion-electron Coulomb energy transfer function (Dermer 1986),
and

$$t_{\rm visc} = \frac{4\pi}{3} m_{\rm i}\, R^{3} \frac{n}{\dot{m}} \qquad (11)$$

where $m_{\rm i}$ is the mass of the ion.

Finally we note that in each case the system is taken to be in steady-state, whereby the accretion and in-fall are constant in time, and thus the neutron production and gamma-ray emission are steady.

2.1. The nuclear reactions

Assuming an initial composition for the accreting plasma, that is some initial fractions of hydrogen and helium (90% H, 10% He in the "normal" case, and 10% H, 90% He in the "helium-rich case", which would correspond to a Wolf-Rayet secondary star companion), we compute the rates of the main nuclear reactions which the ions (the protons, alphas, ^{3}He and ^{2}H nuclei) can undergo:

$$\mathrm{p} + \alpha \longrightarrow {}^{3}\mathrm{He} + {}^{2}\mathrm{H}$$

$$\alpha + \alpha \longrightarrow {}^{7}\mathrm{Li} + \mathrm{p}$$

$$\mathrm{p} + {}^{3}\mathrm{He} \longrightarrow 3\mathrm{p} + \mathrm{n}$$

$$\alpha + \alpha \longrightarrow {}^{7}\mathrm{Be} + \mathrm{n}$$

$$\alpha + {}^{3}\mathrm{He} \longrightarrow \alpha + 2\mathrm{p} + \mathrm{n}$$

$$\mathrm{p} + {}^{2}\mathrm{H} \longrightarrow 2\mathrm{p} + \mathrm{n}.$$

The first two reactions contributing to the destruction of helium (our source of neutrons), and the last four reactions are the actual neutron-producing processes. We disregard

all high-energy neutron-production from proton-proton collisions. The cross sections are essentially the same as those used in Guessoum & Kazanas (1999), and the reaction rates are calculated through the usual non-relativistic expression for binary processes ($r_{ij} = n_i n_j/(1+\delta_{ij}) < \sigma_{ij} v_{ij} >$, the averaging here is performed over thermal distributions for the ions).

We then let the plasma evolve over the dynamical timescale $t_{\rm d}$, with its temperature and density set by the disk structure equations given above for each model, as the material sinks in the gravitational well. We use a simple numerical scheme of explicit finite-differencing to follow the abundances of the various species (the neutrons in particular). This calculation is performed for various values of the model parameters: $\dot{M} = 10^{-10}$, 10^{-9} and 10^{-8} $M_\odot$/yr; $\alpha = 0.3$ and 0.1; $M = 1$; etc. Note that since we are only interested in neutron production in the disk and not in any radiative processes, the electron temperature $T_{\rm e}$, whenever needed, is taken as a free parameter, usually equal to either 100 or 500 keV.

The escape of the neutrons is handled in the same way as in Aharonian & Sunyaev (1984) or Guessoum & Kazanas (1990), that is by computing the fraction of neutrons that have kinetic energies sufficient to overcome the gravitational binding to the compact object: $1/2 m_{\rm n}(v_{\rm flow} + v_{\rm thermal})^2 > GMm_{\rm n}/R$; this translates into a fraction of escaping neutrons given by Eqs. (13)–(15) of Guessoum & Kazanas (1990).

One final important aspect of the neutrons produced is their energy distribution. This aspect was addressed briefly in Guessoum & Kazanas (1999), where it was concluded that a thermal distribution of the neutrons with a temperature equal to that of the ions in the disk is reasonable. This point proves to be important not only for the escape fraction, but also for the interaction of those neutrons that reach the secondary star's atmosphere, since their various interactions there depend strongly on their kinetic energies.

2.2. Neutron production results in various disks

Before presenting results of neutron production for the various disk models, we first show the main characteristics of these models. Figures 1 show the plasma density n (in units of 10^{15} cm^{-3}), the ion temperature $T_{\rm i}$ (in units of MeV), the escape fraction of neutrons $f_{\rm esc}$, and the abundance of neutrons achieved in the disk, all as a function of $r = R/R_{\rm S}$, in the ADAF, ADIOS, SLE, and Uniform-$T_{\rm i}$ (10 and 30 MeV), respectively, for disks with solar composition (90% H and 10% He) and an accretion rate of 10^{-9} $M_\odot$/yr; for ADAF, ADIOS, and SLE the value of α in the figures is 0.1, and for the Uniform-$T_{\rm i}$ models the electron-temperature used for the figures is 0.5 MeV.

Table 1 presents the results of these calculations, showing the rates of neutron production in the ADAF-model case for various values of the viscosity parameter α and the mass accretion rate $\dot{M}$ (1a corresponds to a "normal" composition; 1b corresponds to the "helium-rich" case). All the results shown correspond to $M = 1\,M_\odot$ and $R \approx 100\ R_{\rm S} \approx 10^7$ cm, though the actual results are mostly insensitive to the value of the outer radius of the disk, as most of the nuclear reactions and neutron production take place in the inner part (less than about 10 $R_{\rm S}$) of the accretion flow where the ion temperature is several tens of MeV.

Table 2 is equivalent to Table 1 in the ADIOS model. Table 3 corresponds to the SLE model; Tables 4 and 5 correspond to the uniform-$T_{\rm i}$ model, with $T_{\rm i} = 30$ MeV and $T_{\rm i} = 10$ MeV. Respectively.

It is interesting to note that the resulting neutron fluxes depend strongly on the models considered, but also are quite sensitive to the 3 disk parameters considered, namely α, $\dot{M}$, and the initial composition of the plasma.

Table 1. Neutron production rate (in neutrons/s) in the ADAF Model, for initial **a)** 90% H and 10% He and **b)** 10% H and 90% He compositions.

$\dot{M}$ ($M_\odot$/yr)	a		b	
	$\alpha = 0.3$	$\alpha = 0.1$	$\alpha = 0.3$	$\alpha = 0.1$
10^{-10}	1.1×10^{37}	5.6×10^{37}	6.6×10^{37}	2.7×10^{38}
10^{-9}	4.4×10^{38}	1.4×10^{39}	2.6×10^{39}	6.0×10^{39}
10^{-8}	9.1×10^{39}	1.6×10^{40}	3.9×10^{40}	7.3×10^{40}

Table 2. Neutron production rate in the ADIOS Model, for initial **a)** 90% H and 10% He and **b)** 10% H and 90% He compositions.

$\dot{M}$ ($M_\odot$/yr)	a		b	
	$\alpha = 0.3$	$\alpha = 0.1$	$\alpha = 0.3$	$\alpha = 0.1$
10^{-10}	1.7×10^{37}	1.4×10^{38}	1.4×10^{38}	7.9×10^{38}
10^{-9}	1.6×10^{39}	7.8×10^{39}	9.9×10^{39}	3.5×10^{40}
10^{-8}	8.3×10^{40}	2.3×10^{41}	3.6×10^{41}	9.8×10^{41}

Table 3. Neutron production rate in the SLE Model, for initial **a)** 90% H and 10% He and **b)** 10% H and 90% He compositions.

$\dot{M}$ ($M_\odot$/yr)	a		*b*	
	$\alpha = 0.3$	$\alpha = 0.1$	$\alpha = 0.3$	$\alpha = 0.1$
10^{-10}	3.6×10^{23}	5.0×10^{33}	6.5×10^{24}	8.6×10^{34}
10^{-9}	4.2×10^{36}	2.9×10^{38}	5.0×10^{37}	1.8×10^{39}
10^{-8}	5.0×10^{39}	1.9×10^{40}	3.3×10^{40}	1.3×10^{41}

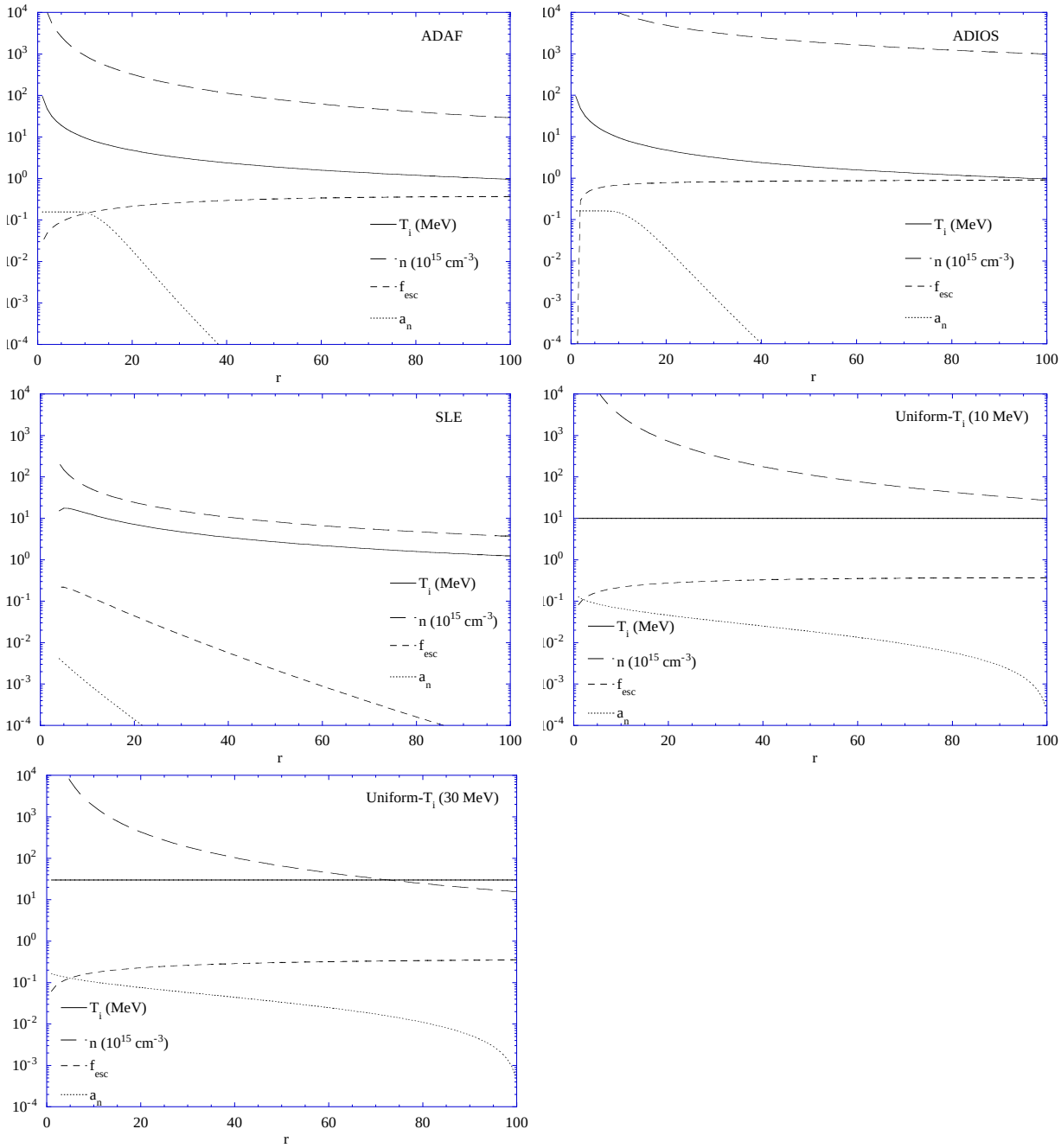

Fig. 1. Plasma characteristics (density, ion temperature, escape fraction of neutrons, and abundance of neutrons) as a function of r, in the ADAF, ADIOS, SLE, and Uniform-$T_{\rm i}$ (10 and 30 MeV), assuming $\dot{M} = 10^{-9}\ M_{\odot}$/yr, $\alpha = 0.1$, and $T_{\rm e} = 0.1$ MeV.

3. Propagation, slow-down and capture of neutrons in the atmosphere of the secondary

A fraction of the neutron flux emitted by the accretion disk irradiates the atmosphere of the secondary star. Some of these neutrons get thermalized; some are captured by nuclei, others decay or escape the secondary if after several scatterings their kinetic energies become larger than the gravitational potential energy binding them to the star. The 2.22 MeV photons resulting from the capture of neutrons by protons escape the secondary atmosphere if they are not absorbed or Compton scattered in the surrounding gas. Consequently, the probability of escape of 2.22 MeV photons depends on the depth of their creation site (in the atmosphere) and on their direction of emission with respect to the surface.

These processes have all been modeled, in the aim of determining the rate of 2.22 MeV radiation emitted by the secondary. The transport of neutrons in the secondary has been simulated using the code GEANT/GCALOR, which takes into account elastic and inelastic interactions as well as the neutrons' decay and capture by nuclei.

Table 4. Neutron production rate in the uniform ion temperature model with $kT_\mathrm{i} = 30$ MeV, for initial **a)** 90% H and 10% He and **b)** 10% H and 90% He compositions.

$\dot{M}$ ($M_\odot$/yr)	a		b	
	kT_e = 0.5 MeV	kT_e = 0.1MeV	kT_e = 0.5 MeV	kT_e = 0.1 MeV
10^{-10}	3.2×10^{38}	4.8×10^{37}	7.4×10^{38}	1.0×10^{38}
10^{-9}	2.4×10^{39}	4.3×10^{38}	6.0×10^{39}	1.0×10^{39}
10^{-8}	1.6×10^{40}	5.1×10^{39}	4.4×10^{40}	3.1×10^{40}

Table 5. Neutron production rate in the uniform ion temperature model with $kT_\mathrm{i} = 10$ MeV, for initial **a)** 90% H and 10% He and **b)** 10% H and 90% He compositions.

$\dot{M}$ ($M_\odot$/yr)	a		b	
	kT_e = 0.5 MeV	kT_e = 0.1 MeV	kT_e = 0.5 MeV	kT_e = 0.1 MeV
10^{-10}	2.0×10^{38}	2.1×10^{37}	4.0×10^{38}	4.1×10^{37}
10^{-9}	1.6×10^{39}	2.1×10^{38}	3.6×10^{39}	4.8×10^{38}
10^{-8}	1.1×10^{40}	1.8×10^{39}	2.7×10^{40}	8.0×10^{39}

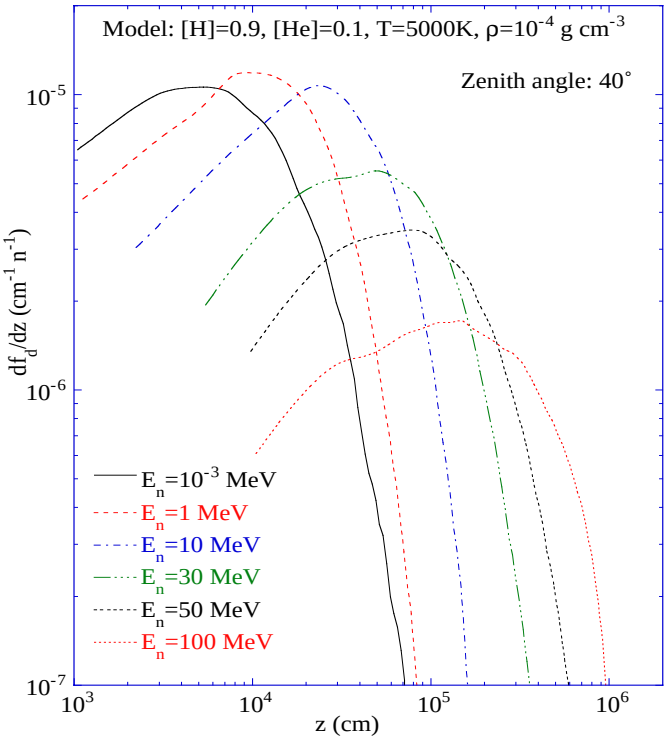

Fig. 2. Distributions of the neutron capture sites in the secondary's atmosphere for several impinging neutron energies.

The radiative transfer of 2.22 MeV photons in the atmosphere and the fraction of neutrons falling back onto the secondary are then modeled separately, using the results of the previous simulations. The total emissivity at 2.22 MeV is estimated by integrating over the whole secondary surface irradiated by neutrons. In the following paragraphs details of the method are presented.

The secondary star has a mass and a radius denoted hereafter by M_s and R_s. (There should be no confusion between the Schwarzchild radius (R_S) of the primary and the radius (R_s) of the secondary star.) The star's atmosphere is characterized by a temperature T_s, a density ρ_s and an abundance in H and in He of [H] and [He], respectively. The isotopic abundance of these elements are taken from Anders & Grevesse (1989). We have disregarded all other elements in the atmosphere. The distance between the accretion disk and the center of the secondary (also called separation) is parametrized by d_s. This distance d_s and the radius of the star determine the fraction of the neutron flux emitted by the accretion disk that irradiates the secondary. The secondary's mass and radius allow us to calculate the gravitational potential and therefore the fraction of escaping neutrons, which also depends on their energy and direction. The temperature, the density, and the composition of the atmosphere are parameters for the simulation of neutron tracks in the secondary. The abundance of ^{3}He is a crucial parameter for the intensity of the 2.22 MeV line emission since, though it is estimated to be $\approx 10^5$ less abundant than H, it has a cross section for neutron capture 1.61×10^4 times that of H. Consequently, this isotope is able to remove neutrons from the atmosphere rather efficiently, thereby reducing the rate of their capture by protons. The density and the composition also determine the mean free path of 2.22 MeV photons in the atmosphere.

Simulations of neutrons with an energy E_n impinging on the atmosphere at a zenith angle ψ have also been performed. For each assumption of E_n and ψ, a depth distribution of neutron capture by H ($\mathrm{d}f_\mathrm{d}(z; E_\mathrm{n}, \psi)/\mathrm{d}z$) and an energy and zenithal distribution of neutrons leaving the atmosphere ($\mathrm{d}F(E, \theta; E_\mathrm{n}, \psi)/(\mathrm{d}E\mathrm{d}\theta)$) are computed. These distributions are normalized to the number of impinging neutrons. Figure 2 shows the depth distribution of the sites of neutron capture by protons for neutrons impinging with an angle of 40 degrees. For neutron energies lower than ≈0.01 MeV, the depth distribution of neutron capture sites and the energy and zenithal distribution of neutrons leaving the atmosphere are rather constant (with respect to energy) for a given initial zenith angle. In fact, at these energies, the neutrons are quickly thermalized in the vicinity of the surface and all follow the same thermal diffusion.

Depending on their energy and direction, some of the neutrons that are ejected out of the atmosphere get decelerated gravitationally and fall back onto the secondary's surface; some of them decay in the process. This fraction ($F_\mathrm{r}(E_\mathrm{n}, \psi)$) of neutrons returning to the atmosphere depends on the energy and zenith angle of the impinging neutrons. Indeed, the larger the neutrons' energy, the deeper they can go, and the smaller the zenith angle

of the impinging neutrons the deeper they will also go. Consequently, the probability for a neutron to leave the atmosphere decreases with increasing energy and decreasing zenith angle. The fraction $F_{\rm r}(E_{\rm n},\psi)$ is calculated using Eq. (19) of Hua & Lingenfelter (1987), which determines the time required for a neutron to return to the atmosphere as a function of its energy and zenith angle. This time is used to determine the fraction of neutrons decaying in flight before they return to the atmosphere. The spectrum of the escaping and returning neutrons has a cut-off value below the escape energy ($E_{\rm n}^{\rm (esc)} = \frac{GMm_{\rm n}}{R} \approx 2\ {\rm keV}\frac{M/M_\odot}{R/R_\odot}$) because even if a neutron has a kinetic energy a little less than the escaping energy, the time spent to return to the atmosphere can be larger than its lifetime.

The angular distribution of the returning neutrons is very close to an isotropic distribution. Simulations have thus been performed to derive the depth distribution of 2.22 MeV creation sites ($\mathrm{d}f_r(z)/\mathrm{d}z$) due to returning neutrons. As previously stated, this distribution is flat for low neutron energies. A fraction $F_{\rm r,0}$ of these returning neutrons can again leave the secondary. However they all return to the atmosphere, since their energies are smaller than the escaping energy, and they can then again undergo one of the following: generate 2.22 MeV photons, decay, be captured by ^{3}He, or leave again the secondary atmosphere (with a fraction given by $F_{\rm r,0}$).

The total depth distribution for the radiative capture of neutrons is obtained by adding to the "direct" depth distribution (without taking into account the returning neutrons) the returning-neutrons component. This component is obtained by calculating the sum of the geometric series of the fraction $F_{\rm r,0}$. The total depth distribution of 2.22 MeV creation site is then:

$$\frac{\mathrm{d}f(z;E_{\rm n},\psi)}{\mathrm{d}z} = \frac{\mathrm{d}f_{\rm d}(z;E_{\rm n},\psi)}{\mathrm{d}z} + \frac{\mathrm{d}f_{\rm r}(z)}{\mathrm{d}z}\frac{F_{\rm r}(E_{\rm n},\psi)}{(1-F_{\rm r,0})}. \quad (12)$$

The angular distribution of the escaping 2.22 MeV photons is computed using the total depth distribution of 2.22 MeV photon creation sites. Let ξ and χ be the zenithal and azimutal direction angles of the 2.22 MeV photon. The angular distribution of escaping 2.22 MeV photons induced by a neutron of energy $E_{\rm n}$ impinging on the atmosphere with a zenith angle of ψ is:

$$\frac{\mathrm{d}\epsilon_{2.2}(\xi,\chi;E_{\rm n},\psi)}{\mathrm{d}\Omega} = \frac{1}{4\pi}\int_z \frac{\mathrm{d}f(z;E_{\rm n},\psi)}{\mathrm{d}z}\,\mathrm{e}^{\frac{-z}{\lambda_{2.2}\cos\xi}}\,\mathrm{d}z \quad (13)$$

with $\lambda_{2.2}$ being the mean free path of 2.22 MeV photons in the secondary's atmosphere. This angular distribution, expressed in photons steradian^{-1} neutron^{-1}, is independent of the azimuth. Figure 3 shows an example of 2.22 MeV photons angular distribution for neutrons impinging with various $E_{\rm n}$'s at a zenith angle of 0°.

The total 2.22 MeV intensity depends on the direction of observation with respect to the binary system frame. Indeed, the 2.22 MeV photons are emitted only from the surface of the secondary that is irradiated by neutrons. Therefore, the observable gamma-ray flux comes only from

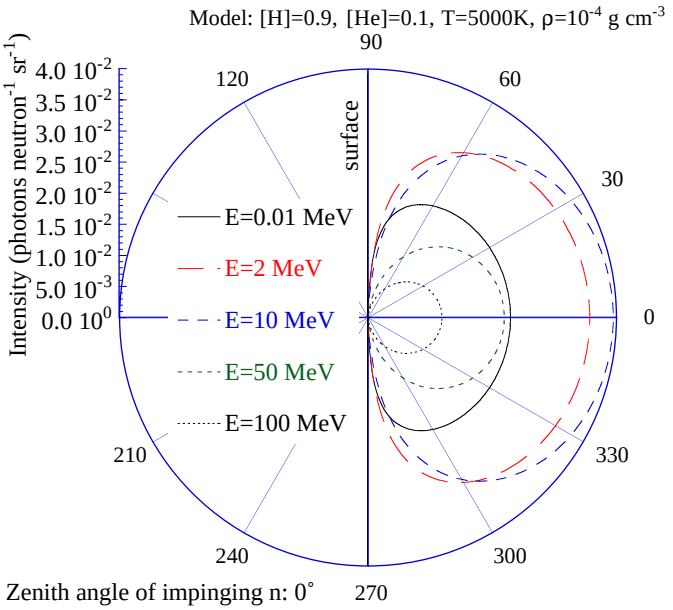

Fig. 3. Angular distributions of the 2.22 MeV photons emitted from the secondary atmosphere for several impinging neutron energies.

the fraction of the secondary area that is irradiated by neutrons and is visible for the observer (see Fig. 4). So we can expect to observe a periodic 2.2 MeV line flux due to the rotation of the binary system. The total 2.22 MeV intensity $I_{2.2}(\alpha,\delta)$ (photons s^{-1} sr^{-1}) in a direction (α, δ) can be obtained by estimating the integral:

$$I_{2.2}(\alpha,\delta) = \frac{N_{\rm n}}{4\pi}\int_D\int_{E_{\rm c}}^{\infty}\frac{\mathrm{d}F(E)}{\mathrm{d}E}\frac{\mathrm{d}\epsilon_{2.2}(\xi,\chi;E,\psi)}{\mathrm{d}\Omega}\mathrm{d}\Omega\mathrm{d}E \quad (14)$$

where $\mathrm{d}F(E)/\mathrm{d}E$ is the energy distribution of neutrons reaching the secondary, $N_{\rm n}$ is the neutron rate (in n s^{-1}) emitted by the accretion disk, φ and θ the direction of the emitted neutrons (see Fig. 4) and D is the integration domain ($\varphi,\theta \in D$) defined as the intersection of the irradiated area (delimited in a cone of angle $\varphi_{\rm max}$) and the visible area in the direction α and δ. In this equation, ξ is a function of φ, θ, α and δ. The zenith angle ψ depends only on φ. The integration domain depends not only on the direction of emission but also on the radius of the secondary and on its distance with respect to the neutron source.

4. Results

We have considered two models for the composition and the geometrical characteristics of the secondary star (see Table 6). The values shown in the table have been chosen so as to compare neutron capture efficiency in helium-enriched and non-enriched ("normal") atmospheres. Calculations of the 2.22 MeV emissivity with specific, accurate secondary star parameters of known binary systems will be presented in a separate publication (Jean et al. 2001, in preparation).

Calculations based on the method presented in the previous section have been performed in the aim of deriving

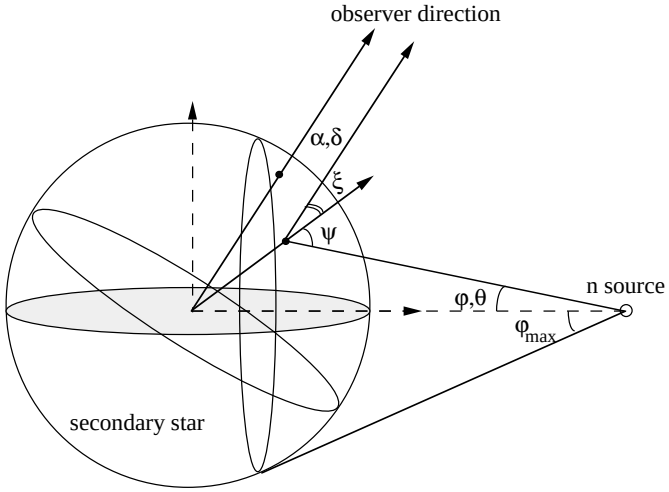

Fig. 4. Schematic view of the irradiation of the secondary star by neutrons. The binary system frame is represented by the dashed axes.

Table 6. Characteristics of the secondary star for the two models.

	Model 1	Model 2
Radius ($R_\odot$)	1	3.6
Mass ($M_\odot$)	1	10
Density (g/cm^3)	10^{-4}	10^{-5}
Temperature (K)	5000	10 000
[H]	0.9	0.1
[He]	0.1	0.9

the expected flux in the 2.22 MeV line from the binary system. The energy distribution of neutrons was assumed to be a Maxwellian with $kT = 10$ MeV, truncated at 5 MeV (E_c in Eq. (14)) because the gravitationnal potential of the primary compact object retains the neutrons of lower energy (see Sect. 2). Since we are dealing with close binary systems, the separation is less than 40 $R_\odot$, which is the mean free path of 5 MeV neutrons in the vacuum. Therefore, the energy distribution does not necessitate an additionnal cut to account for the loss of neutrons by decay during their trip to the secondary star.

4.1. Fraction of escaping 2.22 MeV photons

The fraction of escaping 2.22 MeV radiation ($f_{2.2}$) is defined as the ratio of 2.22 MeV photons that reach the secondary star surface (outward) without scattering to the total number of incident neutrons. This fraction is calculated by integrating the angular distribution of escaping 2.22 MeV photons (see Eq. (4)) over all the possible angles. The 2.22 MeV photons produced by the returning neutrons are also taken into account. The fraction $f_{2.2}$ depends on the zenith angles and energies of incident neutrons. It gives an idea of the efficiency of neutrons in producing an observable 2.22 MeV line. Figures 5 show the escaping 2.22 MeV fraction for the two models of the secondary star. The difference in the neutron capture rate between the two models is principally due to the difference in the composition of the atmosphere. Indeed the abundance of ^{3}He in the second model is such that a large fraction of neutrons are captured by this nucleus and thus lost. Consequently, the neutrons capture rate decreases by a factor ≈17 between the two models. In Model-2 the 2.22 MeV photons are emitted deeper in the atmosphere, and so their shorter mean free path lowers the fraction of escaping photons by a factor 1.5 compared to Model-1. Finally, the gravitational escaping energy of neutrons in Model-2 is slighty lower than in Model-1, increasing the fraction of escaping neutrons and further reducing the 2.22 MeV emissivity in Model-2. All these effects lead to a decrease of $f_{2.2}$ by a factor ≈30 for Model-2 with respect to Model-1 at low E_n.

The fraction of escaping 2.22 MeV photons depends not only on the neutron capture rate but also on the transmission of 2.22 MeV photons in the atmosphere. In Model-1 (see Fig. 5a), where the neutron energy is lower than the escaping energy, the neutrons thermalize quickly and stay in the upper layer of the atmosphere. If they leave the atmosphere, they cannot escape the secondary but a fraction of them decay before returning in the atmosphere. The fraction of escaping neutrons increases with the zenith angle. Indeed, high-zenith-angle incident neutrons can more easily escape since they scatter close to the surface. This is not the case for low-zenith-angle incident neutrons that go deeper in the atmosphere: even if they scatter toward the surface, their energies are rarely above the escape value. This explains why the $f_{2.2}$ fraction decreases with increasing zenith angle below 5 MeV. Above 5 MeV, neutrons penetrate and are captured deeper in the atmosphere. The fraction of escaping neutrons is reduced, as well as the transmission of 2.22 MeV photons. However, for large zenith angles, the neutron captures happen closer to the surface in zones allowing the 2.22 MeV photons to escape more easily from the star.

The variation of the 2.22 MeV photon escaping fraction as a function of the angle and the energy of impinging neutrons in Model-2 is similar to that in Model-1. However, a resonance in the elastic scattering of neutrons with ^{4}He at 1.1 MeV is at the origin of the drop around 1 MeV (see Fig. 5b). At this resonance, the angular distribution of ^{4}He-scattered neutrons is peaked for backward directions[1]. Consequently, around 1 MeV, incident neutrons are more likely to backscatter and to be ejected out of the atmosphere with kinetic energies too high to allow them to return. This effect reduces the number of MeV neutrons that can thermalize and produce 2.2 MeV photons, hence the trough seen in Fig. 5b.

[1] See the ENDF/B-VI evaluated neutron data; `http://t2.lanl.gov/cgi-bin/nuclides/endind`

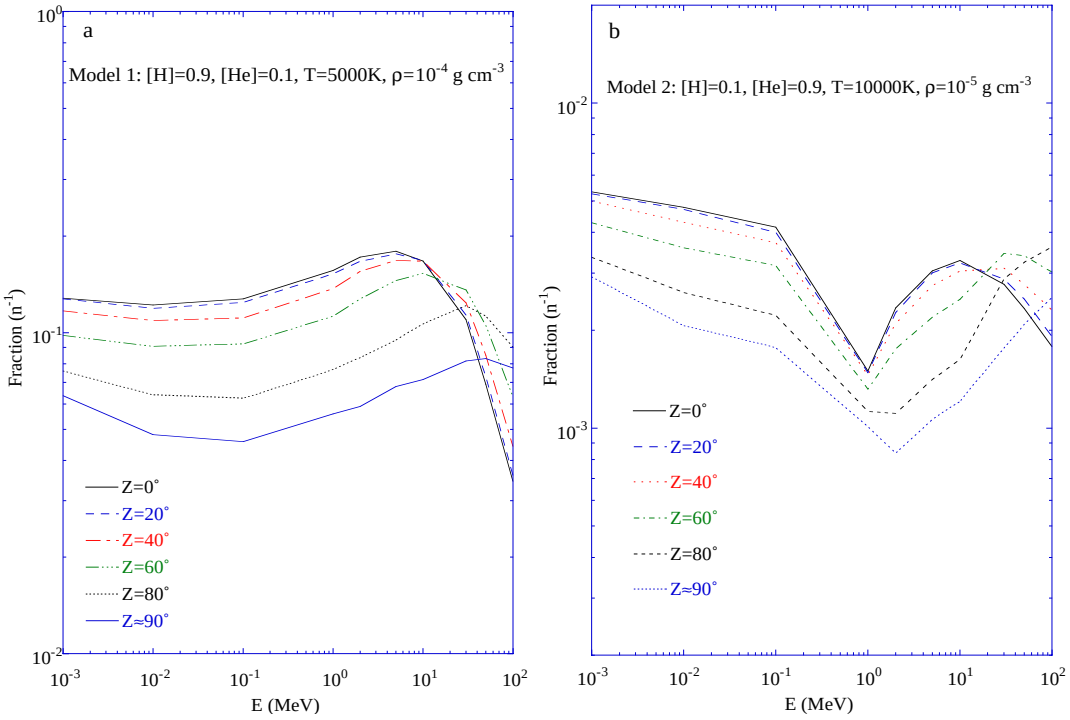

Fig. 5. Fraction of escaping 2.2 MeV photons as a function of the impinging neutron energies for several impinging zenith angle. The two models are presented separately.

4.2. Flux versus model and irradiation geometry

The distance between the accretion disk (the source of neutrons) and the center of the secondary star, and the angles α and δ, which specify the direction of Earth (see Fig. 4), are the basic parameters of this calculation. Since the binary system is rotating, α varies with time and the observed flux becomes periodic. Intensities have been calculated as a function of the direction of emission for different values of the distance between the primary and secondary stars. Assuming parameters of the binary system (separation and masses), it has been possible to derive light curves of the 2.22 MeV line emission, depending on δ. However, the range of interesting separations is limited since the secondary radius needs to fill its Roche lobe in order to allow the accretion of its matter by the compact object. Using a study by Paczynski (1971) that calculated the critical radius of a star in a binary system that allows the outward flow of its matter, we estimated the upper limit of the separation to be between 3.5–6 $R_\odot$ for a secondary star of 1 $M_\odot$ (Model-1) and 7.5–11 $R_\odot$ for a secondary star of 10 $M_\odot$ (Model-2), providing compact object masses ranging from 3 to 20 $M_\odot$. With this type of close binary systems, the period of rotation is less than a day.

Figure 6 shows phasograms of the 2.22 MeV intensity as a function of the separation for Model-1. As expected, the intensity is maximum when the neutron-irradiated area of the secondary star atmosphere faces the observer. The maximum value of the intensity decreases with increasing separation values because the neutrons flux impinging on the atmosphere decreases with increasing

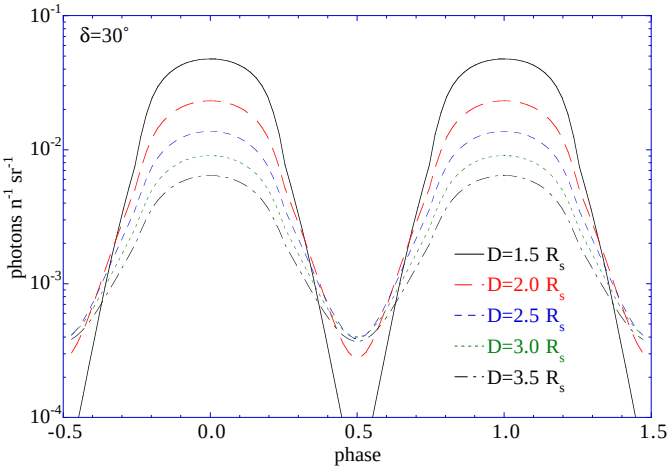

Fig. 6. Example of phasogram of the 2.2 MeV emission for the Model-1 with a compact object mass of 3 $M_\odot$. δ is the angle between the binary system plan and the direction of the observer. D is the distance between the accretion disk and the secondary star in solar radius unit. The period of the binary system change from 0.1 to 0.4 days.

distance between the accretion disk and the secondary. In Fig. 6, the intensity is equal to zero at a phase value of 0.5 only for a separation of 1.5 $R_\odot$, because for this value of δ the irradiated area is hidden by the star. For larger separations, the irradiated area becomes larger and a fraction of this area is always visible by the observer.

The mean and the root-mean-square (rms) fluxes are commonly used for the analysis of periodic emissions. They have been estimated for our 2.22 MeV intensity as

Table 7. Mean 2.22 MeV flux vs. accretion disk models (at 1 kpc for a separation of 2 $R_\odot$ and an initial 90% H and 10% He composition).

Accretion model	$\dot{M}$ ($M_\odot$/yr)	$\alpha = 0.3$	$\alpha = 0.1$
	10^{-10}	1.1×10^{-8}	5.5×10^{-8}
ADAF	10^{-9}	4.3×10^{-7}	1.4×10^{-6}
	10^{-8}	9.1×10^{-6}	1.5×10^{-5}
	10^{-10}	1.6×10^{-8}	1.3×10^{-7}
ADIOS	10^{-9}	1.5×10^{-6}	7.8×10^{-6}
	10^{-8}	8.3×10^{-5}	1.1×10^{-4}
	10^{-10}	3.5×10^{-22}	4.8×10^{-12}
SLE	10^{-9}	4.1×10^{-9}	2.8×10^{-7}
	10^{-8}	4.8×10^{-6}	1.8×10^{-5}
		$kT_e = 0.5$ MeV	$kT_e = 0.1$ MeV
	10^{-10}	3.1×10^{-7}	4.7×10^{-8}
UIT − 30 MeV	10^{-9}	2.3×10^{-6}	4.2×10^{-7}
	10^{-8}	1.6×10^{-5}	4.9×10^{-6}
	10^{-10}	1.9×10^{-7}	2.0×10^{-8}
UIT − 10 MeV	10^{-9}	1.6×10^{-6}	2.0×10^{-7}
	10^{-8}	1.1×10^{-5}	1.7×10^{-6}

Table 8. Mean 2.22 MeV flux vs. accretion disk models (at 1 kpc for a separation of 8 $R_\odot$ and an initial 10% H and 90% He composition).

Accretion model	$\dot{M}$ ($M_\odot$/yr)	$\alpha = 0.3$	$\alpha = 0.1$
	10^{-10}	1.0×10^{-9}	4.0×10^{-9}
ADAF	10^{-9}	3.9×10^{-8}	9.2×10^{-8}
	10^{-8}	6.0×10^{-7}	1.1×10^{-6}
	10^{-10}	2.1×10^{-9}	1.2×10^{-8}
ADIOS	10^{-9}	1.3×10^{-7}	5.2×10^{-7}
	10^{-8}	5.4×10^{-6}	1.5×10^{-5}
	10^{-10}	9.7×10^{-23}	1.3×10^{-12}
SLE	10^{-9}	7.5×10^{-10}	2.7×10^{-8}
	10^{-8}	4.9×10^{-7}	2.0×10^{-6}
		$kT_e = 0.5$ MeV	$kT_e = 0.1$ MeV
	10^{-10}	1.1×10^{-8}	1.5×10^{-9}
UIT − 30 MeV	10^{-9}	9.0×10^{-8}	1.5×10^{-8}
	10^{-8}	6.6×10^{-7}	4.6×10^{-7}
	10^{-10}	6.0×10^{-9}	6.1×10^{-10}
UIT − 10 MeV	10^{-9}	5.4×10^{-8}	7.2×10^{-9}
	10^{-8}	4.1×10^{-7}	1.2×10^{-7}

a function of the separation and the direction of the observer. Both the mean and the rms intensities decrease with increasing separation values as a power law with slope around −2 (between −1.8 and −2.3). Figures 7 and 8 show the variation of the mean and rms intensities as a function of the binary separation for the two models.

The mean intensity does not vary significantly with the angle of the Observer's direction with respect to the binary system plane. The rms intensity decreases, however, showing a reduction of the modulation of the visible photon flux with increasing δ. The modulation obviously disappears for a direction of observation of the binary system perpendicular to the plane of the latter ($\delta = 90^o$).

The flux at 2.22 MeV can be derived using the formula:

$$F_{2.2} = 10^{-5} \frac{R_n}{10^{40}\,\mathrm{n\,s^{-1}}} \frac{I_{2.2}}{10^{-2}\,\mathrm{n^{-1}\,sr^{-1}}} d_{\mathrm{kpc}}^{-2}\,\mathrm{s^{-1}\,cm^{-2}} \quad (15)$$

where R_n is the rate of neutrons emitted by the accretion disk, $I_{2.2}$ is the normalized intensity and d_{kpc} the distance of the binary system to the observer in kpc. For Model-1, the flux at 1 kpc is found to be in the range 10^{-7}–10^{-5} photons s^{-1} cm^{-2} depending on the accretion disk model. For Model-2, it is found to be in the range 10^{-8} to 10^{-6} photons s^{-1} cm^{-2} depending on the accretion disk model. Combining the results of R_n from Sect. 2 (Tables 1a, b to 5a, b) with the calculations in this section, we obtain the final fluxes $F_{2.2}$, which we present succinctly in Tables 7 and 8. The separations have been chosen to be 2 $R_\odot$ and 8 $R_\odot$ for Model-1 and Model-2 respectively, since for these values the mean fluxes do not change significantly with the binary system inclination (see Figs. 7 and 8).

The rotation of the binary system leads to a shift in the centroid of the 2.22 MeV line. This Doppler shift changes with the phase and depends on the observer's direction (δ). Using classical relations in binary systems (e.g. Franck et al. 1992) we derive a relation (Eq. (16)) for the spectral shift of the 2.22 MeV line which depends on the masses of the compact object and the secondary (M_c and M_s, respectively, in solar masses), the separation between the two objects (d_s in solar radii), the phase (ϕ), and the angle between the observer's direction and the binary system (δ).

$$\Delta E = 3.2 \frac{M_c}{\sqrt{d_s(M_c + M_s)}} \cos\delta \sin\phi\ \mathrm{keV}. \quad (16)$$

The estimated spectral shift is mesurable with SPI, the spectrometer onboard the INTEGRAL satellite. Using Eq. (16) and the intensity variation as a function of the phase (as presented in Fig. 6) we have obtained the 2.22 MeV line profiles for Model-1 (Figs. 9) with a compact companion of 3 $M_\odot$ and for two values of the binary system inclination[2]. The line is broadened and double-peaked due to the rotation of the secondary star. Figures 10 show the shape of the line as it could be measured by SPI (assuming a spectral resolution of 2.9 keV at 2.22 MeV). For an inclination of 80° the double-peak shape is clearly visible, whereas for a 10° inclination that is not the case.

[2] The inclination i is the angle between the binary system rotation axis with respect to the observer direction, i.e. $i = 90^o - \delta$.

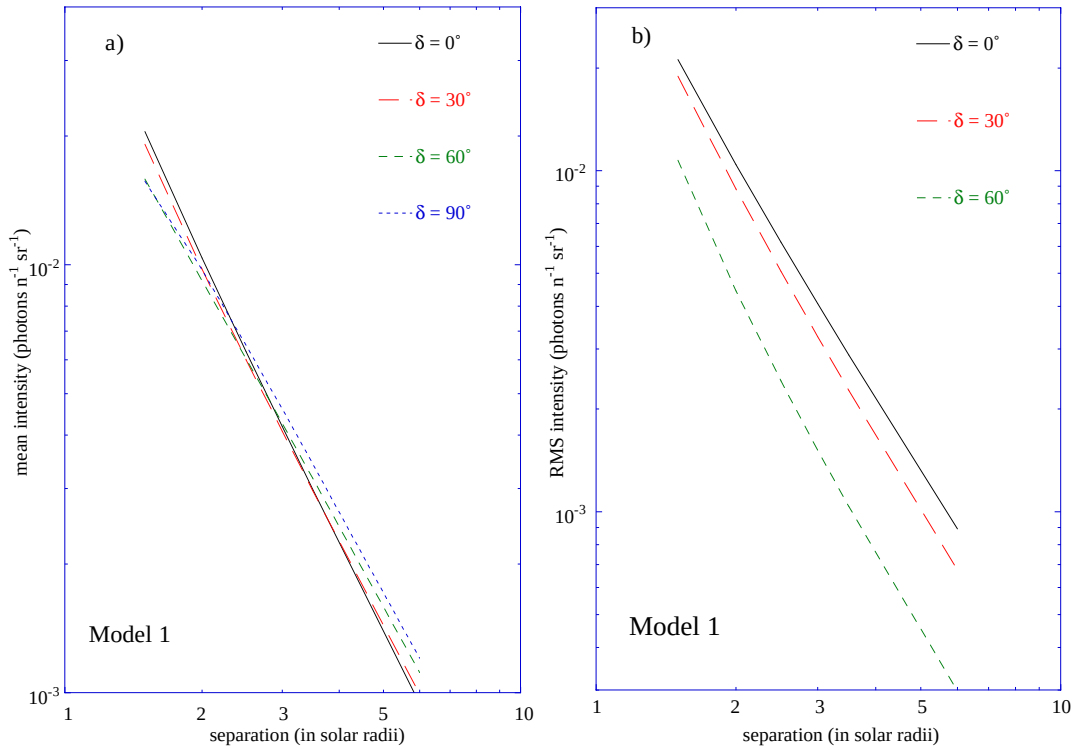

Fig. 7. Normalized mean **a)** and rms **b)** intensities for Model-1 as a function of the separation of the binary. Several values of δ are shown.

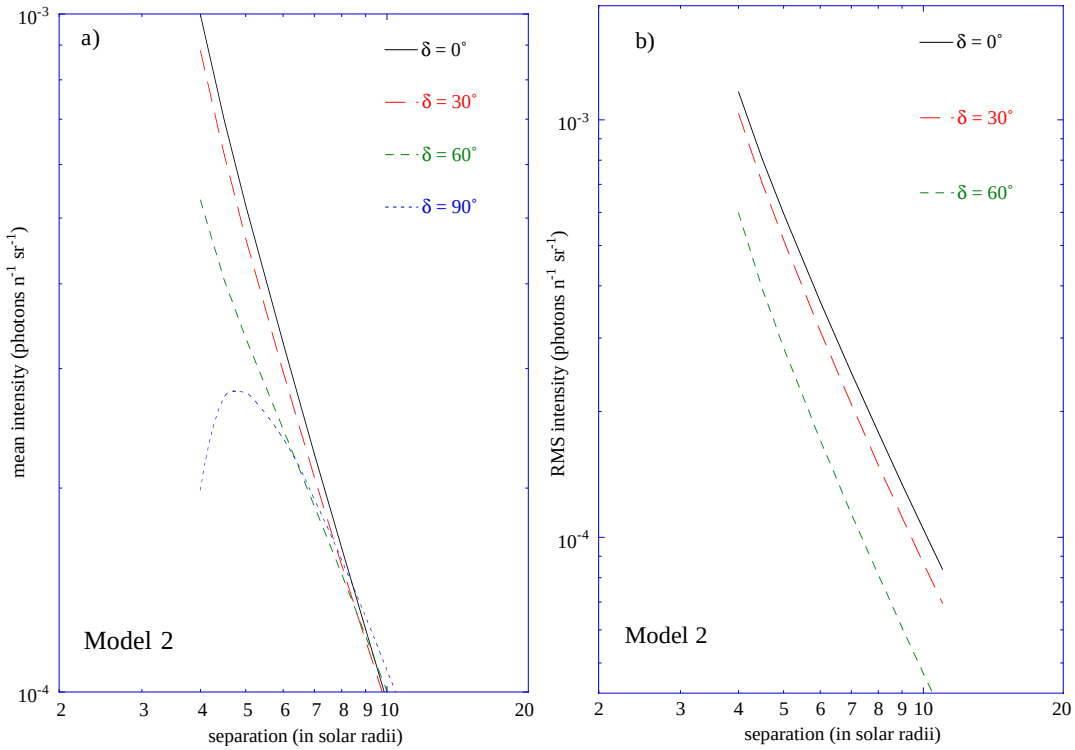

Fig. 8. Normalized mean **a)** and rms **b)** intensities for Model-2 as a function of the separation of the binary. Several values of δ are shown.

5. Conclusions

We have presented a theoretical investigation of the 2.22 MeV line emitted from X-ray binary systems neutrons are captured in the secondary's atmosphere. These neutrons are produced in the accretion disk by nuclear spallation of helium nuclei. The rate of production of neutrons depends on various parameters set by the accretion disk model, i.e. the temperature, density, and

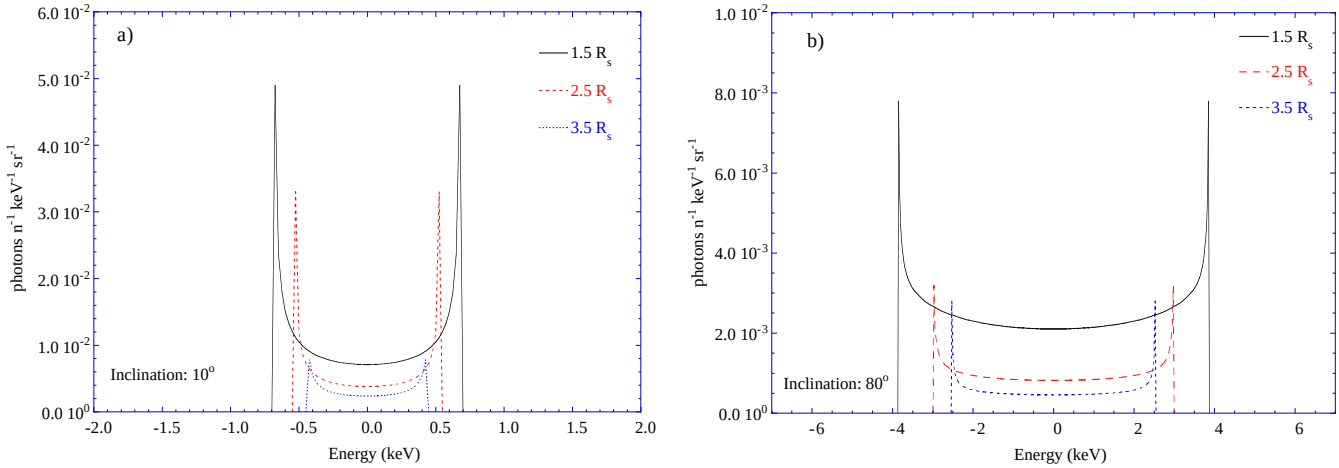

Fig. 9. Shape of the neutron capture line for Model-1. The inclination of the binary system is 10° **a)** and 80° **b)**. Several values of the binary separation are shown.

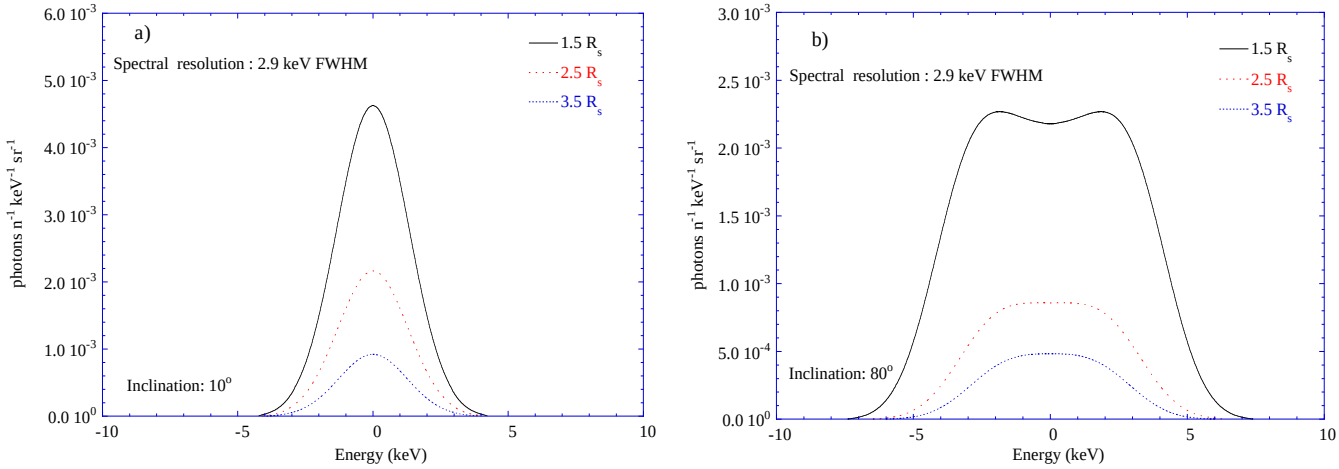

Fig. 10. Estimation of the neutron capture line shape for Model-1 as it could be measured by the spectrometer SPI of INTEGRAL. The inclination of the binary system is 10° **a)** and 80° **b)**. Several values of the binary separation are shown.

composition of the accreted material. Calculations of the line intensity normalized to the neutron production rate have been performed for two simple secondary models and for several X-ray binary geometries.

We showed that, due to the rotation of the secondary, the intensity of the 2.22 MeV radiation is periodic, and the line centroid is shifted by the Doppler effect. The mean intensity does not vary significantly with the direction of observation with respect to the binary system frame.

According to our model, the spectral (Figs. 9 and 10) and temporal (Figs. 6–8) analyses of the 2.22 MeV line flux would provide valuable insights into the characteristics of the binary system (separation, inclination with respect to the observer, masses, accretion rate and disk structure, etc.). If one further knows the X-ray luminosity, the geometry of the X-ray binary system, and its distance from Earth, then a measure of a 2.22 MeV line flux from it can set constraints on the neutron production rate and consequently on the accretion disk models (ADAF, ADIOS, SLE, etc.).

At 2.22 MeV the narrow γ-ray line sensitivity of the SPI spectrometer of the INTEGRAL mission is expected to be 7–10 $\times 10^{-6}$ photons s^{-1} cm^{-2} for an observation time of 10^6 s (Jean et al. 1999). The 2.22 MeV fluxes estimated for the simple secondary-star models and for the various accretion disk models used here are found to be measurable by the spectrometer SPI in some cases: mostly if the accretion rate is large enough ($\dot{M} \approx 10^{-8}\ M_\odot$/yr) and the viscosity is significant ($\alpha \gtrsim 0.2$). In case of a detection, the SPI spectral resolution (≈3 keV at 2.22 MeV) would allow the measurement of the broadening of the line, which is due to the rotation of the secondary, if the separation and the inclination of the X-ray binary are not too large.

In a future work, the 2.22 MeV line flux and shape will be estimated for known X-ray binary systems (e.g. A0620-00, etc.) using all accurate, available information on their characteristics (distance, separation, composition, etc.). The calculated fluxes will be compared with upper-limit fluxes obtained with COMPTEL (Van Dijk 1996), and correlation with other gamma-ray lines will be investigated.

Indeed, the neutrons that irradiate the secondary star can also produce Be and Li isotopes in its atmosphere. This process was proposed by Guessoum & Kazanas (1999) to explain the overabundance of Li in some soft X-ray transients. Both ^{7}Li and ^{7}Be emit gamma-ray lines (at 0.478 and 0.429 MeV), and ^{7}Be decays into ^{7}Li* (with a half-life of 56 days), the latter then produces 0.478 MeV radiation upon de-exciting; such a delayed gamma-ray emission, although weak, would be a clear signature of the process. We can thus expect a certain correlation of the 2.22 MeV emission with these gamma-ray lines, providing supplementary insights into the physics of the binary system.

Acknowledgements. We thank D. Kazanas for his useful comments. N. Guessoum would like to acknowledge a short visiting professor invitation by Université Paul Sabatier and the American University of Sharjah for a summer research grant; he also wishes to thank Prs. P. von Ballmoos and G. Vedrenne for the facilities provided at the Centre d'Étude Spatiale des Rayonnements (Toulouse, France) where much of this work was conducted.

References

Anders, E., & Grevesse, N. 1989, Proc. AIP Conf., Minneapolis, NY, 1–8
Aharonian, F. A., & Sunyaev, R. A. 1984, MNRAS, 210, 257
Bildsten, L. 1991, in Gamma-Ray Line Astrophysics, ed. P. Durouchoux & N. Prantzos, AIP Conf. Proc. 232 (New York: AIP), 401, 615
Bykov, A. M., et al. 1999, Astro. Lett. Comm., 38, 285
Blandford, R. D., & Begelman, M. C. 1998, MNRAS, 303L, 1
Chen, X., et al. 1995, ApJL, 443, 61
Dermer, C. D. 1986, ApJ, 307, 47
Fichtel, C. E., & Trombka, J. I. 1981, Gamma-Ray Astrophysics, NASA SP-453
Franck, J., King, A. R., & Raine, D. J. 1992, Accretion Power in Astrophysics (Cambridge University press)
Guessoum, N., & Dermer, C. D. 1988, in Nuclear Spectroscopy of Astrophysical Sources, ed. N. Gehrels, & G. H. Share, AIP Conf. Proc. 107 (New York: AIP), 332
Guessoum, N., & Kazanas, D. 1990, ApJ, 358, 525
Guessoum, N., & Kazanas, D. 1999, ApJ, 512, 332
Harris, M. J., & Share, G. H. 1991, ApJ, 381, 439
Hua, X. M., & Lingenfelter, R. E. 1987, ApJ, 323, 779
Hua, X. M., & Lingenfelter, R. E. 1987, Solar Phys., 107, 351
Jacobson, A. S., et al. 1978, Gamma-Ray Spectroscopy in Astrophysics (NASA T.M. 79619), 228
Jean, P., et al. 1999, in The Fifth Compton Symposium, ed. M. L. McConnell, & J. M. Ryan, AIP Conf. Proc. 510 (New York: AIP), 708
Kazanas, D., Hua, X.-M., & Titarchuk, L. 1987, ApJ, 480, 735
McConnell, M., et al. 1997, in Proc. of the Fourth Compton Symposium, ed. C. D. Dermer, M. S. Strickman, & J. D. Kurfess, AIP Conf. Proc. 410 (New York: AIP), 1099
Murphy, R. J., et al. 1991, ApJ, 371, 793
Narayan, R., & Yi, I. 1995, ApJ, 428, L13
Narayan, R., & Yi, I. 1995, ApJ, 452, 710
Narayan, R., Yi, I., & Mahadevan, R. 1995, ApJ, 374, 623
Paczynski, B. 1971, ARA&A, 9, 183
Ramaty, R., et al. 1995, ApJ, 455, L193
Ramaty, R., Mandzhavidze, N., & Kozlovzky, B. 1996, in High Energy Solar Physics, ed. R. Ramaty, N. Mandzhavidze, & X. M. Hua, AIP Conf. Proc. 374, (New York: AIP), 172
Shapiro, S. L., Lightman, A. P., & Eardley, D. M. 1976, ApJ, 204, 187
Share, G. H., & Murphy, R. J. 1995, ApJ, 452, 933
Van Dijk, R. 1996, Ph.D. Thesis, 148
Vestrand, W. T. 1989, in Proceedings of the Gamma-Ray Observatory Workshop, ed. N. Johnson, 4-274
Yi, I., & Narayan, R. 1997, ApJ, 486, 363